INT. J. REMOTE SENSING, 1988, VOL. 9, NO. 5, 1013–1022

Dependence of image grey values on topography in SIR-B images

G. DOMIK† and F. LEBERL

VEXCEL Corporation, 2905 Wilderness Place, Boulder, Colorado 80301, U.S.A.

and J. CIMINO

Jet Propulsion Laboratory, California Institute of Technology,
Pasadena, California 91109, U.S.A.

Abstract. This paper focuses on the use of a high resolution digital elevation model (DEM) to aid in rectifying and enhancing synthetic aperture radar images. Using a synthetic backscatter image, the SIR-B images are manually rectified and resampled to remove geometric distortions caused by topography. In a second step, an improved reflectance function of incidence angle is derived from the DEM and the rectified image and this function is used to reduce radiometric effects of topography yielding an albedo image which clearly shows the thematic, as opposed to topographic content of the image. The procedure is tested on four SIR-B images of a scene in Argentina (crossover point) that is imaged under different azimuth and incidence angles. The similarity of the resulting images indicates that the procedure effectively reduces artefacts from the images that are dependent on topography.

1. Introduction

One difficulty in working with synthetic aperture radar imagery is that the appearance of the scene is heavily dependent on azimuth (flight orientation) and incidence angles (defined as the angle between radar beam and surface normal). First, areas of high elevation in imaged terrain are displaced toward the sensor in the image. Secondly, the backscatter of terrain sloped toward the sensor is augmented; this causes these areas to be brighter in the image. If the sensor is oriented in different directions, the brightness of different parts of the imaged scene will be increased from one image to another.

The objective of this investigation was to separate thematic information from topographic information in order to derive an enhanced image that can be more easily interpreted. This involves resampling the image to correct for geometric distortion and locally rescaling grey values to remove the variation in backscatter that is caused by terrain undulations. Such images are easier to compare by highlighting thematic information.

2. Test area

A set of four overlapping SIR-B images was the basis of the present investigations, a continuation of radargrammetric studies of SIR-B imagery over Argentina (see Leberl *et al.* 1986 a, b, Domik *et al.* 1986, Cimino *et al.* 1986). Two images each from descending and from ascending orbits are combined using a set of geometrically and radiometrically rectified images. Access to aerial photography led to the creation of a

† Present address: Center for Astrophysics and Space Astronomy, University of Colorado at Boulder, Boulder, Colorado 80309-0391, U.S.A.

north is toward the top of the page. The upper pair originates from the descending orbit and the lower pair originates from the ascending one.

Ascending and descending orbits crossed at an angle of approximately 86°, hence they are almost perpendicular to one another. Because radar enhances features perpendicular to the illumination direction, images from ascending and descending orbits are difficult to merge visually with each other. Two distinct features help to orient the images, the town of José de San Martin (bright backscatter in descending images) and a cinder cone-shaped mountain due north of the town.

Aerial photographs were available at a scale 1:80 000. They were used to collect elevation data covering most of the test site in the form of 25 m contour lines and they were rastered to a DEM (see figure 2 for a perspective view of the area). Use of a 512 by 512 pixel image processor made it necessary to reduce the original SIR-B image resolution from 12·5 m per pixel to 37·5 m in order to process all of the overlap area. A mean filter was used for the image reduction. The raster size of the DEM was also chosen to be 37·5 m.

3. Geometric preprocessing of digital images

The rectification process applied here has been described repeatedly in previous publications (e.g. Domik *et al.* 1986). It differs from straightforward warping with control points or from differential rectification with a DEM in that we employ a simulated radar image to make the network of ground control data more dense. Other approaches to geometric rectification have been presented by Naraghi *et al.* (1983), Guindon *et al.* (1981), Kwok and Curlander (1987) and others.

Geometric distortions in radar images are caused mostly by topographic variation of the imaged terrain. Therefore the use of a DEM is essential in removing these distortions, known as foreshortening and layover. The amount of distortion is also influenced by imaging parameters such as elevation angle, defined as the angle between a line from sensor position to nadir and the radar beam. Consequently, precise

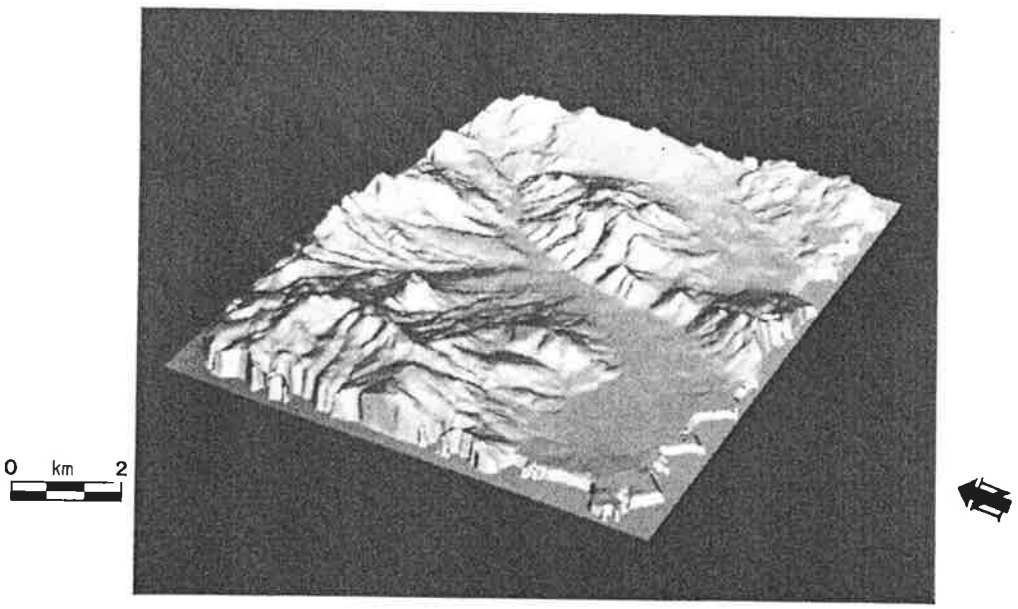

Figure 2. DEM (digital elevation model) derived from aerial photography and displayed as perspective view. The size of the area is approximately 18 km × 14 km.

knowledge of orbit and imaging parameters is critical to the accuracy of a geometric rectification.

In this paper the radar images were rectified using elevation data from aerial photography. This was preferred over using elevation models derived from SIR-B data because of the increased detail that could be obtained from aerial photography.

In the first step of the rectification process a synthetic radar image is created utilizing the DEM, available orbit/imaging parameters and a radar backscatter curve derived by Muhleman (1964). During this procedure a link is established between the synthetic image grey values and the grid cells of the DEM and is stored for further use. The resulting simulated radar image resembles the actual Synthetic Aperture Radar image. We proceed by identifying match points between the synthetic and real radar image (see figure 3) based on a visual inspection by an operator using shadows, edges, etc. These match points are used together with ground control points to warp the real radar grey values to the ideal radar geometry of the synthetic radar scene. A second resampling step utilizes the stored links between radar grey value and DEM grid cell by placing each radar image pixel into the geometry of the DEM (ortho-image geometry).

The four resulting ortho-images from various orbits are easily comparable on a visual and on a pixel-by-pixel basis as a result of the geometric fidelity. Figure 4 shows the ortho-image of one descending data take. Comparison with Figure 1 (*a*) demonstrates the effect of geometric rectification.

4. Scatter plots of grey values versus incidence angles

During geometric rectification, the radar grey values were registered to the grid cells of a DEM. Therefore the rectification procedure established a link between incidence angles and grey values. It is then possible to plot grey values as a function of incidence angle for any region of the image (see figure 5). Figure 4 outlines the borders of what is used as the overall image area and subareas in this study.

Subarea A represents the town of José de San Martin. Subarea B shows topographically varied terrain with mostly homogeneous vegetation cover which leads to scatter plots indicating a dependency mainly on terrain slope.

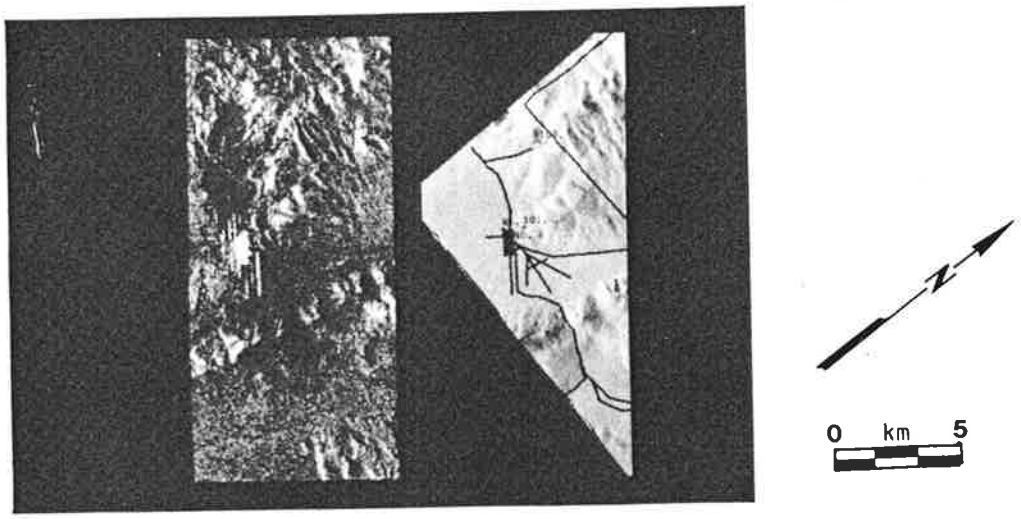

Figure 3. Visual comparison of real and simulated radar image and identification of match points.

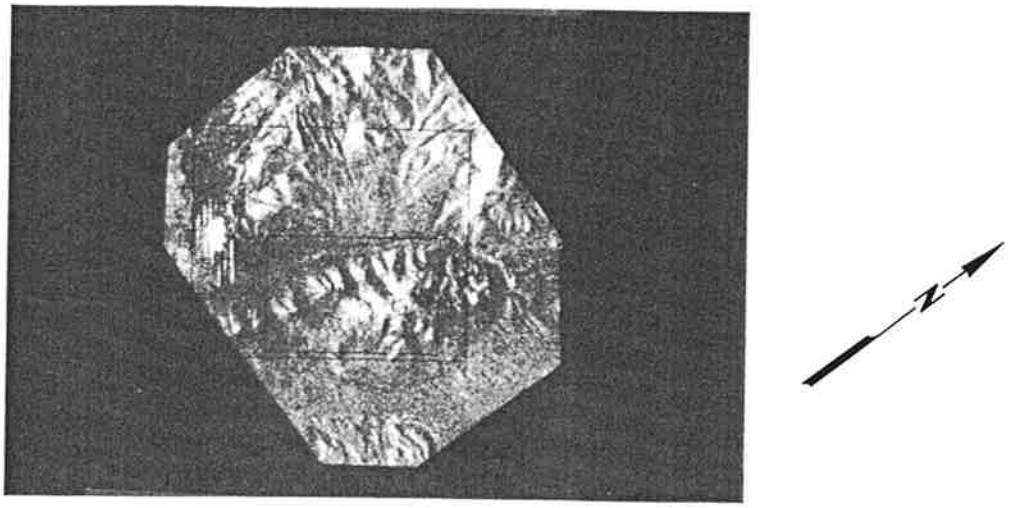

Figure 4. Radar ortho-image of data take 56.4. The black rectangle around the town identifies subarea A, the rectangle to the right of it subarea B and the big rectangle the overall image for derivation of grey value scatter plots.

The scatter plot in figure 5 (*a*) shows the sampled relationship between incidence angle and grey value for the overall area (data take 56·4). The scatter plot is divided into two components in figures 5 (*b*) and (*c*). Figure 5 (*b*) shows the component arising from the town (subarea A). The incidence angle is uniform because the town is built on a flat area and the wide variation in grey values shows the wide variation in backscatter that urban features give rise to; indicating that this area has a different backscatter function than does the rest of the scene. Figure 5 (*c*) shows the scatter plot for subarea B; a relationship between incidence angle and grey level is clearly discernible here.

One way to derive a backscatter curve statistically is to plot the mean grey value for each incidence angle. Figure 5 (*d*) depicts this curve for the sample in figure 5 (*c*). This curve resembles that derived by Muhleman (1964) but is specific to the type of vegetation cover found in the image.

Figure 6 presents the scatter plots of data takes (DTs) 72.4, 92.8 and 76.8, respectively. It can be observed that images taken at different azimuth angle, but similar incidence angle (compare plot 5 (*d*) to 6 (*b*) or plot 6 (*a*) to (*c*)) exhibit a great deal of similarity in their average backscatter plots.

5. Slope-effect reduction

The amount of radar signal scattered back from the ground is dependent on, among other factors, the incidence angle and thematic characteristics of the reflecting target. The influence of the incidence angle (dependent on slope and elevation angle) is rather strong and usually overpowers the thematic variation of the illuminated areas. This is particularly evident in topographically varied terrain.

To interpret grey values in terms of varying thematic influence, it is desirable to reduce the effect of terrain slope, or incidence angle, on the resulting image grey values. This is attempted in the following algorithm.

Geometric rectification indices a geometric correspondence between radar ortho-image and illuminated DEM, where the illumination is derived from an average backscatter curve as in Figure 5 (*d*). When superimposing the rectified image and the illuminated DEM, the areas where the topographic influence surpasses the thematic

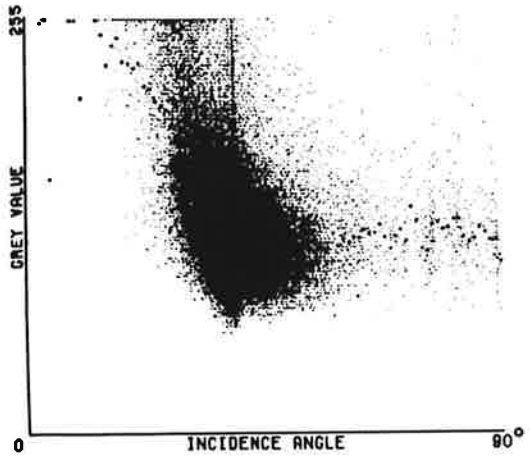

(*a*)

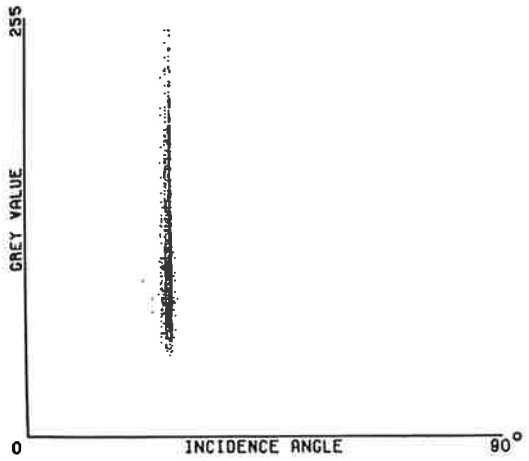

(*b*)

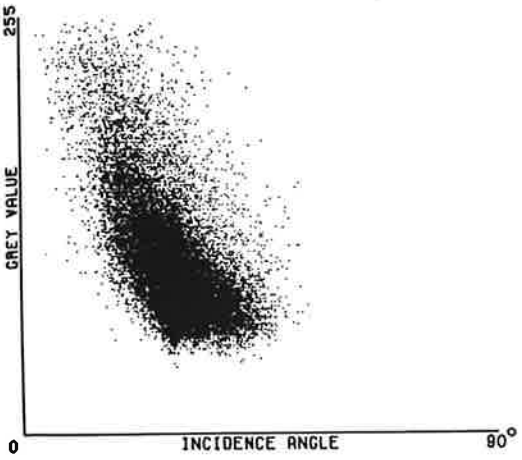

(*c*)

Figure 5. Grey value/incidence angle scatter plots: (*a*) of overall area, bright points indicate average curve; (*b*) of subarea A; (*c*) of subarea B and (*d*) average curve based on (*a*).

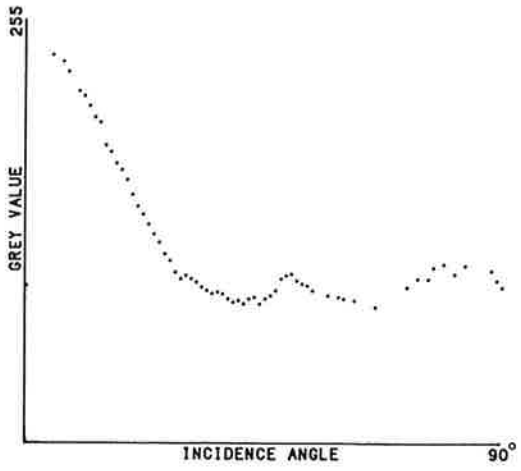

(*d*)

Figure 5 (*continued*)

influence match well (mountainous areas). In areas where the thematic influence is very strong (e.g. towns, rivers, etc.) a mismatch between the grey values of the two files occurs. By taking the difference of the grey values in the illuminated DEM and ortho-image, areas that are alike in their brightness obtain grey values of or close to 0 and areas that mismatch receive distinct grey values in the positive or negative range between 1–255. The variance of the grey values in the difference image denotes, among lesser influences from other factors, microrelief (small scale variation in topography not accounted for in DEM) and thematic content (not accounted for in the average grey value curve). If the equation used for each pixel in this process is

$$\text{radar ortho-image} - \text{illuminated DEM} = \text{difference image}$$

then the resulting grey values in the range $-255 \leqslant \sigma < 0$ indicate that the real grey value was lower than expected from the slope at this pixel, while a grey value $0 < \sigma \leqslant 255$ indicates that the real grey value was brighter than expected from the slope in this point. After slope effect reduction, minor effects should be due to incidence angle. Grey value variations should mainly correspond to thematic content.

Figure 7 presents the four slope effect reduced images of the DTs previously shown in Figure 1. In order to display the differences as an 8-bit image (grey values 0–255), value 0 was shifted to 128 and the total range of values -255 to $+255$ is rescaled into the interval 0–255.

Visual inspection shows details in the data that vary from image to image. This may be due to various effects such as (1) thematic detail, in particular in flat areas, e.g. the town José de San Martin, (2) lack of detail in the DEM and thus a lack of detailed rectification and (3) remaining thematic effects in the mountains, e.g. vegetation differences on north and south slopes, or on slopes exposed to wind.

Figure 8 is an example for the average relationship between the incidence angles and grey values of the slope effect reduced image of DT 56.4. The average curve shows the monotonous trend we were expecting from the monotonous vegetation cover in that area. It is evidence that the slope effect reduction was successful.

(*a*)

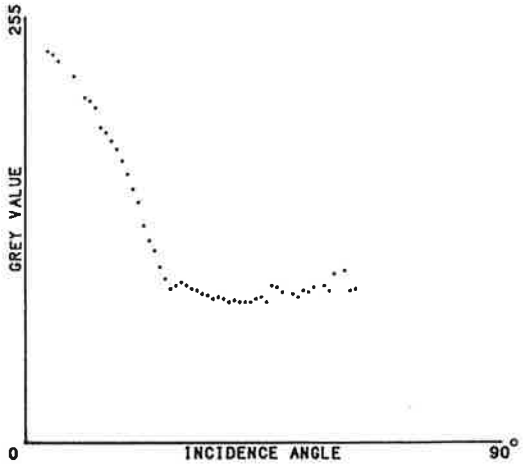

(*b*)

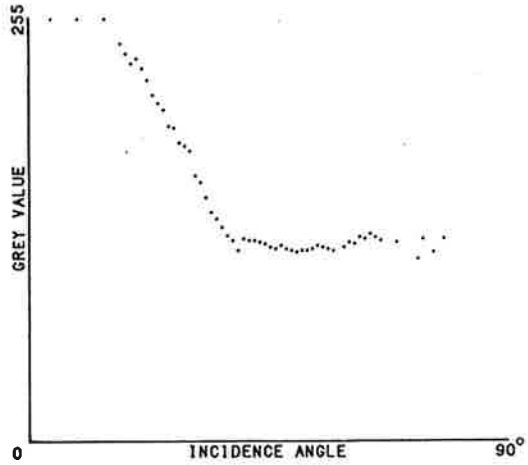

(*c*)

Figure 6. Comparison of average curves relating incidence angles to image density numbers: (*a*) DT 72.4; (*b*) DT 92.8, and (*c*) DT 76.8.

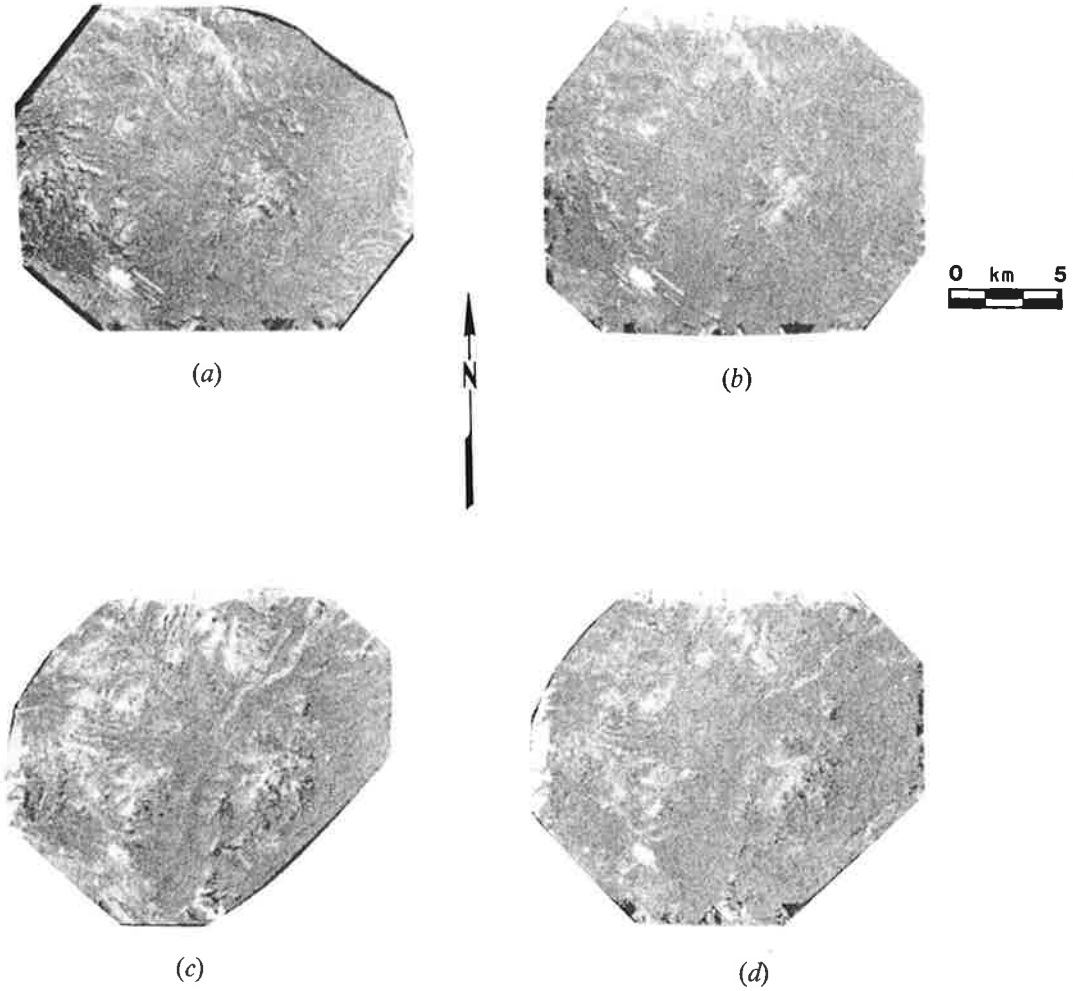

Figure 7. Slope effect reduced SIR-B image segments. (*a*) DT 56.4, (*b*) DT 72.4, (*c*) DT 96.8 and (*d*) DT 76.8.

Figure 8. Slope effect reduced radar images of homogenous areas display a monotonous (average) grey value curve for all incidence angles.

6. Conclusions

The José de San Martin SIR-B radar images provide views of the same scene at different azimuth and incidence angles on topographically varied terrain. These images thus provide a unique test case for an algorithm to remove the effects of topography and incidence angle from a radar image and enhance the thematic content of the image. One would excpect that the similarity of the images would be enhanced by the algorithm if it is successful.

The algorithm provides a method of deriving the backscatter curve for the scene statistically. However, examination of the data revealed that urban features had a different backscatter function from the rest of the image so the samples arising from these areas were removed before the backscatter function was derived.

After the images were rectified and slope effects were reduced with the algorithm, the similarity of the images was indeed enhanced. However, there were residual differences attributable to lack of detail in the DEM and the difference in appearance of thematic elements, such as urban features, under different azimuth angles and variation in the backscatter curve not encompassed by the overall backscatter model.

Acknowledgments

The authors wish to thank Dr. Aldo Brandani who provided the aerial photography of the SIR-B crossover area and E. Kienegger, who produced perspective DEM views. Thanks also to Annie Holmes for providing us with images and parameters. The contributions by Vexcel Corporation to the work for this paper were performed under Contract No. 757549, Subtask 'José de San Martin' for the Jet Propulsion Laboratory.

References

CIMINO, J. B., BRANDANI, A., CASEY, D., RABASSA, J., and WALL, S. D., 1986, Multiple incidence angle SIR-B experiment over Argentina: mapping of forest units. *I.E.E.E. Transactions on Geoscience and Remote Sensing,* **24,** 498–509.

DOMIK, G., LEBERL, F. W., and CIMINO, J. B., 1986, Multiple incidence angle SIR-B experiment over Argentina: generation of secondary image products. *I.E.E.E. Transactions on Geoscience and Remote Sensing,* **24,** 492–497.

GUINDON, G., GOODENOUGH, D. G., and TEILLET, P. M., 1981, The role of digital terrain models in the remote sensing of forests. *Proceedings of the 7th International Symposium Machine Processing of Remotely Sensed Data held in June 1981.*

KWOK, R. and CURLANDER, J., 1987, Automated rectification and geocoding of SAR imagery. *Proceedings of the 1987 International Geoscience and Remote Sensing Symposium held in Ann Arbor, Michigan* (Ann Arbor: Environmental Research Institute of Michigan), pp. 353–355.

LEBERL, F. W., DOMIK, G., RAGGAM, J., and KOBRICK, M., 1986a, Radar stereomapping techniques and application to SIR-B images of Mt. Shasta. *I.E.E.E. Transactions on Geoscience and Remote Sensing,* **24,** 473–481.

LEBERL, F. W., DOMIK, G., RAGGAM, J., CIMINO, J. B., and KOBRICK, M., 1986b, Multiple incidence angle SIR-B experiment over Argentina: stereo-radargrammetric analysis. *I.E.E.E. Transactions on Geoscience and Remote Sensing,* **24,** 482–491.

MUHLEMAN, 1964, Radar scattering from Venus and the Moon. *Astronomical Journal,* **69,** 34.

NARAGHI, M., STROMBERG, W., and DAILY, M., 1983, Geometric rectification of radar imagery using digital elevation models. *Photogrammetric Engineering and Remote Sensing,* **49,** 195–199.

high accuracy digital elevation model (DEM) to be used for the rectification and grey value analysis.

The area subject to this investigation is situated in the Province of Chubut, Argentina, where descending and ascending paths of the Shuttle crossed (approximately 44° 15′ S, 70° 35′ W). The site is named after the town José de San Martin, situated in the crossover area.

The table gives an overview of orbit and imaging parameters and of image quality of the available SIR-B images. Incidence angles as well as azimuth angles differ. This promised to provide a wide range of data suitable for information extraction by comparing the images with each other. Unfortunately the quality of the images limited comparison to some extent; with increasing incidence angle the quality decreased. This has caused some problems throughout the analytical processes. The variation of quality is clearly reflected in the signal-to-noise ratios which range from 7·4 to 4·2 (see table).

Figure 1 shows the overlap area of the four available images, all oriented so that

SIR-B images in the crossover area.

Data take (DT) ·	Scene	Orbit	Centre incidence/ look angle (°)	Quality	Signal-to-noise ratio (dB)
92·8	2	Ascending	31·4/28·3	Good	7·4
76·8	2	Ascending	43·3/39·65	Mediocre	5·4
56·4	11	Descending	32·9/30·3	Good	7·4
72·4	3	Descending	44·7/41	Mediocre	4·2

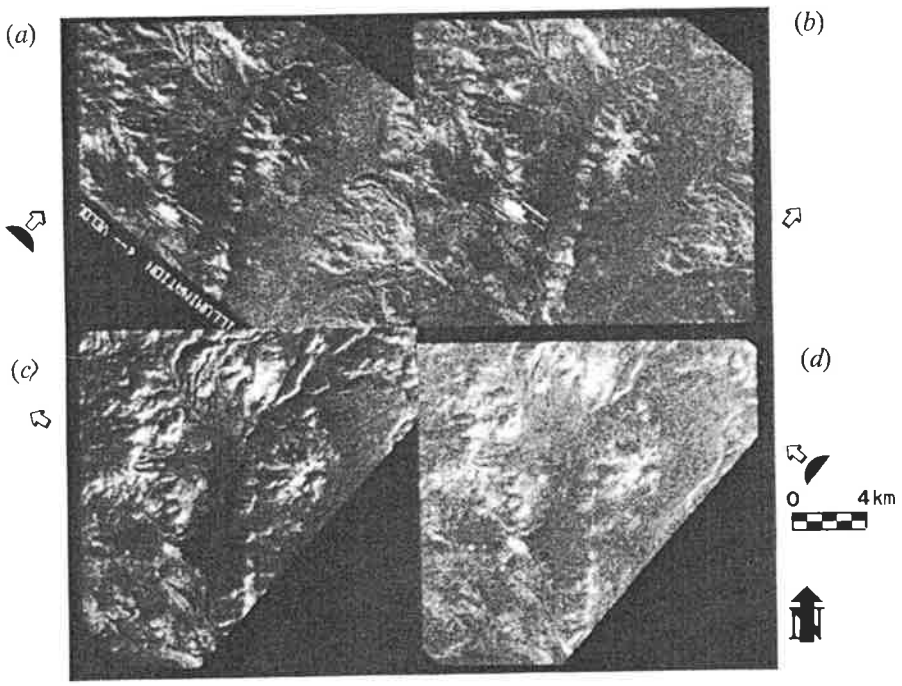

Figure 1. SIR-B images of crossover area in Argentina. Upper pair originates from descending orbits (flight path north-west to south-east); lower pair originates from ascending orbits (south-west to north-east). SIR-B was a left-side-looking system. North is straight up. (*a*) DT 56·4, (*b*) DT 72·4, (*c*) DT 92·8 and (*d*) DT 76·8.

6. Conclusions

The José de San Martin SIR-B radar images provide views of the same scene at different azimuth and incidence angles on topographically varied terrain. These images thus provide a unique test case for an algorithm to remove the effects of topography and incidence angle from a radar image and enhance the thematic content of the image. One would excpect that the similarity of the images would be enhanced by the algorithm if it is successful.

The algorithm provides a method of deriving the backscatter curve for the scene statistically. However, examination of the data revealed that urban features had a different backscatter function from the rest of the image so the samples arising from these areas were removed before the backscatter function was derived.

After the images were rectified and slope effects were reduced with the algorithm, the similarity of the images was indeed enhanced. However, there were residual differences attributable to lack of detail in the DEM and the difference in appearance of thematic elements, such as urban features, under different azimuth angles and variation in the backscatter curve not encompassed by the overall backscatter model.

Acknowledgments

The authors wish to thank Dr. Aldo Brandani who provided the aerial photography of the SIR-B crossover area and E. Kienegger, who produced perspective DEM views. Thanks also to Annie Holmes for providing us with images and parameters. The contributions by Vexcel Corporation to the work for this paper were performed under Contract No. 757549, Subtask 'José de San Martin' for the Jet Propulsion Laboratory.

References

Cimino, J. B., Brandani, A., Casey, D., Rabassa, J., and Wall, S. D., 1986, Multiple incidence angle SIR-B experiment over Argentina: mapping of forest units. *I.E.E.E. Transactions on Geoscience and Remote Sensing*, **24**, 498–509.

Domik, G., Leberl, F. W., and Cimino, J. B., 1986, Multiple incidence angle SIR-B experiment over Argentina: generation of secondary image products. *I.E.E.E. Transactions on Geoscience and Remote Sensing*, **24**, 492–497.

Guindon, G., Goodenough, D. G., and Teillet, P. M., 1981, The role of digital terrain models in the remote sensing of forests. *Proceedings of the 7th International Symposium Machine Processing of Remotely Sensed Data held in June 1981.*

Kwok, R. and Curlander, J., 1987, Automated rectification and geocoding of SAR imagery. *Proceedings of the 1987 International Geoscience and Remote Sensing Symposium held in Ann Arbor, Michigan* (Ann Arbor: Environmental Research Institute of Michigan), pp. 353–355.

Leberl, F. W., Domik, G., Raggam, J., and Kobrick, M., 1986a, Radar stereomapping techniques and application to SIR-B images of Mt. Shasta. *I.E.E.E. Transactions on Geoscience and Remote Sensing*, **24**, 473–481.

Leberl, F. W., Domik, G., Raggam, J., Cimino, J. B., and Kobrick, M., 1986b, Multiple incidence angle SIR-B experiment over Argentina: stereo-radargrammetric analysis. *I.E.E.E. Transactions on Geoscience and Remote Sensing*, **24**, 482–491.

Muhleman, 1964, Radar scattering from Venus and the Moon. *Astronomical Journal*, **69**, 34.

Naraghi, M., Stromberg, W., and Daily, M., 1983, Geometric rectification of radar imagery using digital elevation models. *Photogrammetric Engineering and Remote Sensing*, **49**, 195–199.